Insights into solute effects on elastic moduli in bcc Fe based solid solutions from first-principles

Wei Liu[a], Xiangyan Li[a], Yange Zhang[a], Xuebang Wu[a], Yichun Xu[a,*], Changsong Liu[a,*], Qianfeng Fang[a], Yunfeng Liang[b,a], Caetano R. Miranda[c]

[a] *Key Laboratory of Materials Physics, Institute of Solid State Physics, Chinese Academy of Sciences, P. O. Box 1129, Hefei 230031, P. R. China*

[b] *Research into Artifacts, Center for Engineering (RACE), the University of Tokyo, Chiba 277-8568, Japan*

[c] *Instituto de Física, Universidade de São Paulo, CP 66318, São Paulo, SP 05315-970, Brazil*

Abstract

Understanding the underlying mechanisms on how solutes modify elastic moduli of metals is essential in numerous areas spanning solid-state physics to materials selection in mechanical design. We perform first-principles calculations to study the elastic moduli changes relative to α-Fe for bcc Fe-based solid solutions, as solute content increases from 0.4 at.% to 1.85 at.%. Besides the "common expectation" that the elastic moduli vary linearly with solute content in these homogeneous solid solutions, nonlinear variations are also observed in Fe-Mn system, which is attributed to the change in electronic environment of Fe solvent rather than in magnetic moment of solute Mn. At the elastic moduli linear regime, solutes modify the bulk modulus B and the polycrystalline shear modulus G through variations in the valence electron density n_{WS} at boundary of Wigner-Seitz cells and the bonding strength, respectively. Interestingly, it is found that with increasing solute content, the change rate of $n_{\mathrm{WS}}^2 V_{\mathrm{m}}$ (V_{m}: mole volume) increases exponentially with the change rate of B, while the change rate of Debye temperature

[0] *Author to whom correspondence should be addressed. Email address:csliu@issp.ac.cn, xuyichun@issp.ac.cn

increases linearly with the change rate of G. For $3d$ transition-metal solutes, the change rate of G with solute content increases linearly with electron-to-atom ratio e/a from Ti to Mn, but decreases linearly with e/a from Co to Cu.

Keywords: Fe based solid solution; elastic modulus; solute effect; underlying mechanism; density functional theory

1. Introduction

In modern industries, body-centered cubic (bcc) Fe based alloys are widely used for load bearing, i.e., in strain state, because of low costs and good mechanical properties. For the past several decades, ferritic and martensitic steels have been investigated for serving under extreme conditions, such as irradiation, corrosion and high temperature. Hereinto, reduced activation ferritic and martensitic steels have been studied as structural materials in the fusion and the next generation fission energy systems [1–5]. Ferritic stainless steels have been considered as promising candidates for interconnects in solid oxide fuel cells [6–9]. Heat-resistant ferritic and martensitic steels have been investigated as superheater materials in fossil fuel power plants [10, 11]. Generally speaking, these variants of ferritic and martensitic steels are produced by: i) adding alloying elements for solid-solution and the second-phase strengthening, ii) dispersing nanoscale oxide particles for improving high-temperature strength and irradiation resistance, and iii) surface modifying and coating for mitigating oxidation and corrosion. Efforts have been made in the research of strain effects on the microstructural evolution, and on the ultimate mechanical properties of ferritic and martensitic steels for applications under extreme conditions. It was demonstrated that in metallic systems, the stability and mobility of solutes are significantly affected by strain [12–15], which might play an important role in radiation-induced segregation. It

was also indicated that the applied strain greatly changes the oxidation rate of metals [16, 17]. Knowing the molecular mechanisms on how the solutes modify the elastic properties of α-Fe can be helpful to predict strain states of ferritic and martensitic steels serving as load-bearing components. This can be used to guide us for better composition design of this class of steels.

The effects of solutes on elastic properties in metallic solid solutions have been extensively studied [18–20, 23–28]. Miedema *et al.* suggested an empirical relationship between bulk modulus (B) and valence electron density (n_{WS}) at the boundary of Wigner-Seitz cells for elemental metals, i.e., $n_{\mathrm{WS}} \sim \sqrt{B/V_{\mathrm{m}}}$, where V_{m} is mole volume [19]. Li and Wu found it applicable to binary intermetallic compounds and suggested the model: $B = n_{\mathrm{WS}}^2 V_{\mathrm{m}}$ [20]. This relation was verified in dilute binary alloys by first-principles calculations [21, 22, 27]. It is reasonable that the surface area A_{WS} of Wigner-Seitz cell approximately scales as $2/3$ power of its volume. From this, it might be deduced an interesting relation: $B \sim n_{\mathrm{WS}}^2 A_{\mathrm{WS}}^{3/2}$, which points out that B is determined by the surface properties of Wigner-Seitz cells in metals. Also based on first-principles calculations, Hu *et al.* reported that for W based solid solutions, the shear modulus along [111] direction is positively related to the electronic charge density between cations in this direction [27]. Many studies revealed the correlations between the change of elastic moduli of metals due to alloying and the electronic properties, the volumetric variation, the relaxation of bond length, as well as the elastic properties of solutes in pure states (see a summary in later Table 5) [21, 22, 27–32]. It might be concluded that solutes modify the elastic properties of matrix metals by the combination effects of volumetric and chemical bonding changes [28, 31, 32]. Theoretical evidences indicated that the addition of solutes with higher B in pure states usually results in higher B of the metallic solid solutions; but when those solutes with lower B in pure states are added, the metallic solid solutions usually have lower B

[21, 22, 29]. These studies certainly improve our understanding of solute effect on elastic properties of metallic solid solutions. However, the underlying mechanism of how solutes modify elastic moduli of α-Fe is still unclear up to now.

Early experiments revealed a linear relation of elastic modulus versus solute content in bcc Fe based solid solutions [33]. Based on experimental results, some studies were done on the correlations between elastic moduli and other properties for Fe-base solid solutions [28, 34]. It was found that the rates of change of polycrystalline shear modulus G and Young's modulus E with composition depend on the change of lattice parameter with composition and upon the position of the solute in the periodic table [34]. Ghosh and Olson decomposed the solute effect on G into two contributions: the electronic and the volumetric [28]. They found a systematic trend in the electronic contribution as a function of electron-to-atom ratio (e/a). Additionally, several theoretical studies on elastic moduli of bcc Fe based solid solutions have been done [24, 25, 32, 35–37]. By using all-electron exact muffin-tin orbital (EMTO) method in combination with coherent potential approximation (CPA), Zhang *et al.* calculated the single-crystal and polycrystalline elastic moduli of ferromagnetic bcc Fe-X (X = Al, Co, Cr, Mg, Mn, Ni, Rh, Si, V) random solid solutions [35–37]. Based on first-principles theory with CPA, Khmelevska *et al.* studied the variations of B with solute content in bcc $Fe_{1-c}X_c$ (X=Si, Ge, Sn; $0 < c < 0.25$) disordered solid solutions [24]. Their calculations including magnetic properties provide an explanation for the experimental non-monotonous variation of B with solute content in Fe-Si system. Fellinger *et al.* proposed an efficient method for computing solute-induced changes in lattice parameters and elastic stiffness coefficients C_{ij} of single crystals using density functional theory [32]. However, theoretical studies to elucidate the solute effect on elastic moduli of bcc Fe based solid solutions are still needed, to check the conventional concepts and to provide new insights.

In this paper, first-principles calculations are performed to obtain elastic moduli for 12 bcc Fe based binary solid solutions with solute content from 0.4 at.% to 1.85 at.%. To construct these Fe based solid solution systems, we dope a wide variety of substitutional solutes, including nonmetal Si, simple metal Al, a spectrum of 3*d* transition metals (Ti, V, Cr, Mn, Co, Ni and Cu), and heavy refractory metals (Nb, Mo and W), which have important implications on iron and steel research either theoretically or for engineering applications. In this work, the evolution of electronic structure and magnetism are carefully examined to seek the underlying cause for the variation of elastic moduli versus solute concentration. We investigate the correlations of the solute effect on elastic moduli, with the solute effects on volume, chemical bonding and valence electron density in bcc Fe based solid solutions, and with some intrinsic properties of the solutes.

2. Methodology

All first-principles calculations within Density Functional Theory (DFT) are performed by using Vienna *ab initio* simulation package (VASP) [38], and the detailed settings can be found in Ref. [39]. Bcc Fe based solid solutions with five different solute concentrations are implemented by five periodic supercells that each has one solute besides Fe atoms. The dimensions of these supercells and the corresponding *k*-point meshes are listed in Table 1. Evidently, solutes are perfectly uniform-distributed in bcc Fe matrix in periodic $3 \times 3 \times 3$, $4 \times 4 \times 4$ and $5 \times 5 \times 5$ supercells. It should be noted that solutes are not "absolutely" uniform-distributed in $Fe_{71}X_1$ and $Fe_{95}X_1$ systems implemented respectively by periodic $3 \times 3 \times 4$ and $4 \times 4 \times 3$ supercells, since the number density of solutes in [001] direction is not equal to that in [100] and [010] directions for the two systems. For example, in the case of $Fe_{71}X_1$ system ($3 \times 3 \times 4$ supercell), the number density of solutes is 1/4u in [001] direction, while it is 1/3u in [100] and [010] directions. Herein

"u" denotes unit cell. As a result, $Fe_{71}X_1$ and $Fe_{95}X_1$ systems in equilibrium state are actually in body-centered tetragonal (bct) lattice in this work. However, these bct lattices are verified to be very close to bcc by the following calculations on $Fe_{71}Ti_1$ and $Fe_{95}W_1$ systems. After full structure optimizations on the two systems by simultaneously relaxing the shape, volume and ions, it is found that the length ratio of [001] edge versus [100] (or [010]) edge deviates only slightly from $4/3$ and $3/4$, respectively for $Fe_{71}Ti_1$ and $Fe_{95}W_1$ systems. The relative deviations are both less than 0.1%. Furthermore, when NS1 (SS89) strain is applied on [010] and [001] edges of the two systems [39], no matter the [001]/[010] length ratio is set to $4/3$ (for $Fe_{71}Ti_1$) and $3/4$ (for $Fe_{95}W_1$), or equilibrium values, the calculated C' (C_{44}) shows very small variation, and the relative difference is less than 2.0%. These results indicate that the elastic properties of the $Fe_{71}X_1$ and $Fe_{95}X_1$ systems can be approximately regarded in bcc symmetry in this work. Therefore, it is a safe approximation that $Fe_{71}X_1$ and $Fe_{95}X_1$ systems are both in bcc lattice. For simplicity, the length ratio of [001] edge versus [100] (or [010]) edge is set to be $4/3$ and $3/4$ for $3 \times 3 \times 4$ and $4 \times 4 \times 3$ supercells, respectively.

In this paper, an arithmetic scheme is employed to extract single-crystal elastic moduli of bcc Fe based solid solutions from first-principles calculated stresses [39]. Table 2 presents some components of strains HS1, HS2, NS1 and SS89, which are applied on all supercells in our calculations. C' is calculated by the equation: $C' = (\sigma_{22} - \sigma_{11})/[2(e_{22} - e_{11})]$. Other equations for calculating single-crystal and polycrystalline elastic moduli can be found in Ref. [39] and references therein. From Ref. [40], the elastic Debye temperature Θ is proportional to a mean elastic wave velocity v_m: $\Theta = h/k \cdot (3/(4\pi\Omega))^{1/3} \cdot v_m$, where h is Planck's constant, k is Boltzmann's constant, and Ω is the atomic volume. In isotropic polycrystals, we can consider the relations: $\rho v_l^2 = B + 4G/3$, $\rho v_t^2 = G$ and $3/v_m^3 = 1/v_l^3 + 2/v_t^3$, where ρ is the mass density, and v_l and v_t are the velocities corresponding to longitudinal

and transverse elastic waves, respectively. Since the input values of B and G are at 0 K, the obtained Θ is equivalent to that associated with lattice specific heat at low temperature limit.

3. Results

Experimental measurement of the effect of uniform-distributed solute at dilute concentration on elastic moduli of α-Fe might be difficult due to the solute-solute and solute-defect clusters [32, 41, 42], and the probable solute nitride as well as carbide complexes [43]. However, it is convenient to construct a metallic solid solution with uniform-distributed solute in molecular modelling [44], so that "pure" solute effect on elastic moduli of α-Fe can be theoretically calculated. This makes possible to disentangle the contributions on the correlations of the solute effect on elastic moduli of α-Fe with the solute effects on other properties of α-Fe, and with the intrinsic properties of a solute. In this work, the polycrystalline elastic moduli at each solute concentration are subtracted by the counterparts of α-Fe simulated with the same group of supercell and k-point mesh, to avoid the systematic error due to different k-point mesh. The polycrystalline elastic moduli of α-Fe simulated with different group of supercells and k-point meshes are listed in Table 3. The calculated differences, ΔB, ΔE and ΔG of Fe-X (X= 12 solutes) systems, representing the changes of elastic properties owing to solutes, are presented on the left panel in Figs. 1 and 2. As it can be seen, for 11 Fe-X (X=Ti, V, Nb, Cr, Mo, W, Co, Ni, Cu, Al and Si) systems, these elastic moduli decrease linearly in different slopes, when solute content increases from 0.4 at.% to 1.85 at.%. As shown in Fig. 1(g), for Fe-Mn system, ΔB increases abruptly and drastically at 1.39 at. % Mn, while ΔG and ΔE increase linearly with Mn content.

The calculated lattice constant changes Δa ($\Delta a = a - a_0$) owing to solutes, are presented on the right panel in Figs. 1 and 2 for all systems. Δa values are

calculated by a of Fe based solid solutions subtracting a_0 of α-Fe simulated with the same group of supercell and k-point mesh (see Table 3), to avoid the influence of different k-point mesh. As we can see, for 10 Fe-X (X=Ti, V, Nb, Cr, Mo, W, Co, Ni, Cu and Al) systems, Δa increases linearly in different slopes when solute content c increases from 0.4 at.% to 1.85 at.%. However, Δa of Fe-Mn and Fe-Si systems show very small change as c increases. It should be noticed that Δa of Fe-Mn system shows an appreciable deviation from the fitting line, at 1.39 at. % Mn. Additionally, the change of Debye temperature, $\Delta\Theta$, of these Fe-X (X= 12 solutes) systems, are calculated in a similar way. As shown on the right panel in Figs. 1 and 2, $\Delta\Theta$ of Fe-Mn system increases linearly with Mn content, while $\Delta\Theta$ of all other systems decreases linearly with solute content.

4. Discussion

4.1. Electronic origin of the nonlinear variation of B with Mn content

It is long established that elastic moduli of bcc Fe based solid solutions with uniformly or randomly distributed solute are linear functions of solute content within solubility limit [28, 32–34]. This model is well confirmed by our calculated ΔG, ΔE and ΔB of 11 dilute bcc Fe-X (X= Ti, V, Nb, Cr, Mo, W, Co, Ni, Cu, Al and Si) systems. However, it is not followed by the ΔB of Fe-Mn system. This linear behavior can be understood for atomic configurations with nonexistence of solute-clusters, impurities and defects. However, the condition from the electronic structure perspective has not been discussed so far. Noticeably, the nonlinear jumps of ΔB and Δa in Fe-Mn system are synchronous, as shown in Figs. 1 (g and g′). In the following part of this subsection, we deduce the necessary condition in electronic structure for the linear dependence of lattice constant a on solute content c in metallic solid solutions, and demonstrate that it is also correct for the linear dependence of bulk modulus B on c.

In a metallic solid solution $M_{1-c}S_c$, the atomic volume Ω, defined as the mean volume per atom, usually varies in a linear fashion with c:

$$\Omega = (1-c)\Omega_{\mathrm{M}} + c\Omega^*_{\mathrm{S}}. \tag{1}$$

Herein, Ω_{M} is the atomic volume of matrix metal M, and Ω^*_{S} is the effective atomic volume of solute S. For some metallic solid solutions, this linear relation is only valid below a maximum solute content c_{max}, since the constant parameter Ω^*_{S} changes when $c > c_{\mathrm{max}}$. According to King's explanation, as solute content c increases beyond c_{max}, sufficient amount of solutes alter the electronic environment of the solvent, leading to the change of the effective solute volume Ω^*_{S} [50]. This implies that the invariance of the electronic environment of the solvent is a necessary condition for the linear dependence of Ω on c. In a dilute bcc Fe based solid solution, the lattice constant a varies linearly with solute content c on the condition that c is below a certain limit c_{max}:

$$a = a_0 + cr_a \qquad c \leq c_{\mathrm{max}}, \tag{2}$$

where a_0 is the lattice constant of α-Fe and r_a is the change rate. Obviously, for a dilute metallic solid solution, cr_a is very small compared with a_0. If one takes the third power on both sides of Eq. (2), and omits those terms of higher than one power of cr_a on the right side, there is

$$a^3 = (1-c)a_0^3 + c(a_0 + 3r_a)a_0^2. \tag{3}$$

After both sides of Eq. (3) are divided by two, it is identical with Eq. (1). We obtain: $\Omega = a^3/2$, $\Omega_{\mathrm{M}} = a_0^3/2$, and $\Omega^*_{\mathrm{S}} = (a_0 + 3r_a)a_0^2/2$. When c increases beyond c_{max}, r_a changes so that a deviates from the linear trend and the linear relation of Ω versus c also breaks down according to Eqs. (2) and (3). Therefore, the nonlinear variation of a with c has the same electronic origin as that of Ω

in dilute Fe based solid solutions, and the linear dependence of a on c implies a necessary condition in electronic structure as that of Ω.

Towards understanding the electronic origin of nonlinear variation of bulk modulus B with c in dilute bcc Fe_{1-c}-Mn_c system, we examine the evolution of differential charge density ρ^{diff} in (110) plane with c in 8 Fe-X (X=Ti, Cr, W, Mn, Co, Ni, Cu and Si) systems. Herein, ρ^{diff} is defined as the difference between the total charge density of a system and the superposition of the isolated atomic charge density placed at atomic sites [45]. One can observe that the ρ^{diff} around solute Mn changes when its content increases from 1.04 at. % to 1.39 at. %, as shown in Fig. 3. For example, the isodensity olive ring transforms from cross-like shape into rhombus-like shape. This clearly shows the electronic environment change around Mn, which leads to the nonlinear variations of ΔB and of Δa with Mn content. On the other hand, we could not observe any variation in ρ^{diff} pictures of (110) plane in other systems as solute content c increases, whose ΔB and Δa are both in linear dependence on c. These results confirm the above deduction that in homogeneous metallic solid solutions, the invariance of electronic environment of solvent is a necessary condition for the linear dependences of B and of a on solute content c. Specifically, once sufficient solutes alter the electronic environment of bcc Fe solvent, the "sensitive" bulk modulus varies nonlinearly at this solute content.

Now, let us turn our discussion on the perspective of the evolution of magnetism in these bcc Fe based solid solutions as solute content c increases from 0.4 at.% to 1.85 at.%. Herein, the magnetic moments of ions are calculated in equilibrium volume, by using the standard Wigner-Seitz radii in the VASP pseudopotential database. The magnetic moments of solutes and Fe ions do not change significantly with c in 7 Fe-X (X=Ti, Cr, W, Co, Ni, Cu and Si) systems, except in Fe-Mn system. Figure 4(a) displays that Fe ions in the nearest two and farther

neighbor shells (1nn, 2nn and farther) around Mn exhibit very small variation of magnetic moment μ, within this range of Mn content; furthermore, the μ values of the 1nn and 2nn Fe ions are slightly smaller than that of farther Fe ions. These results are in good consistence with the experimental conclusion that the magnetic moments of neighboring Fe ions are almost not affected by solute Mn [46]. As shown in Fig. 4(b), the μ of Mn increases monotonously from $-1.84\ \mu_B$ to 0.36 μ_B, as Mn content increases from 0.4 at.% to 1.85 at.%. The magnetized localized state of Mn in ferromagnetic iron was firstly deduced by Jaccarino *et al.* from experiments [47, 48]. The calculated μ of Mn is 0.11 μ_B at 1.39 at.% Mn, which agrees well with the experimental result, nearly zero, in a bcc Fe-Mn solid solution with 1.5 at.% Mn [46–49]. Our calculated μ of Mn is $-1.56\ \mu_B$ in $Fe_{127}Mn_1$ system (0.78 at.% Mn) with lattice constant of 2.8323 Å. This result is very close to the EMTO result, $-1.49\ \mu_B$, but in a large difference with the PAW-PW91 one, 0.9 μ_B, in $Fe_{127}Mn_1$ system reported by Olsson *et al.* [41]. We specially set the lattice constant to 2.83 Å for $Fe_{127}Mn_1$ system, and the calculated μ of Mn, 0.56 μ_B, is roughly consistent with the result of Olsson *et al.* Nonetheless, this volume effect on magnetism of Fe-Mn system might need further research. The Δa variation with Mn content c in Fe-Mn system might be attributed to the μ change of Mn. For example, when c changes from 0.4 at.% to 0.78 at.%, Δa shows a "large" increase, by 0.0011 Å (see Fig. 4(c)), which might be owing to stronger magnetic repulsion among Mn ions due to denser population. Furthermore, it is owing to the smallest magnetic repulsion between Mn and other cations, that Fe-Mn system has the minimum volume at 1.39 at.% Mn. However, this magneto-volume effect may not fully take in account the observed elastic moduli changes in this dilute Fe-Mn system, in view of the predicted hydrostatic-strain effect on elastic moduli of α-Fe in Ref. [31]. For example, from 1.04 at.% Mn to 1.39 at.% Mn, 1) the elastic moduli do not increase uniformly, e.g., 2.20 GPa of ΔC_{44} versus 17.18 GPa

of ΔC_{11}, as shown in Fig. 4(d), which do not indicate a hydrostatic-strain origin; 2) the B increment of 17.67 GPa can not be induced by the very small change of lattice constant, -0.00185 Å, equivalent to hydrostatic-strain decrease of -0.002. Therefore, the nonlinear variation of B, C_{11} and C_{12} can only be attributed to the change of electronic structure in the dilute bcc Fe-Mn system.

4.2. Exponential relation between $\partial(n_{WS}^2 V_m)/\partial c$ and B_{mf}

King defined an atomic volume size factor for metallic solid solutions [50],

$$\Omega_{sf} = \frac{1}{\Omega_{\mathrm{M}}} \cdot \frac{\partial \Omega}{\partial c}. \tag{4}$$

Herein, c denotes solute content; Ω and Ω_{M} are atomic volumes of metallic solid solution and of solvent matrix, respectively. Ω_{sf} expresses the relative change rate of atomic volume with solute content c, and characterizes the solute effect on atomic volume of the solvent [41, 50]. Similarly to Ω_{sf}, an elastic modulus factor can be defined for bcc Fe based solid solutions:

$$\kappa_{mf} = \frac{1}{\kappa_{\mathrm{Fe}}} \cdot \frac{\partial \kappa}{\partial c}. \tag{5}$$

Herein, κ_{Fe} and κ represent elastic moduli of α-Fe and of bcc Fe based solid solution, respectively. κ_{mf} expresses the relative change rate of elastic modulus with solute content c, and characterizes solute effect on an elastic modulus of α-Fe. We will discuss correlations between the solute effect on an elastic modulus of α-Fe and other quantities via κ_{mf} in the following part. Since Debye temperature Θ reflects bonding strength of a crystal [51, 52], its "modulus" factor, Θ_{mf}, is proposed to characterize the solute effect on bonding strength of α-Fe.

Interestingly, let us consider the correlations between the effect of solute on B and some other quantities. Figure 5(a) indicates no correlation between B_{mf} and Θ_{mf} in these dilute bcc Fe based solid solutions. As shown in Fig. 5(b), there is a very weak positive correlation between B_{mf} and Ω_{sf}, which is inconsistent with

the concept that volume expanding leads to decreasing elastic modulus [31, 32, 39]. However, it should be noted that there are good negative correlation between B and equilibrium atomic volume in face-centered cubic (fcc) Al based, bcc W based and hexagonal close-packed (hcp) Mg based solid solutions [22, 27, 29]. Our results show that solute effects on bonding strength and on volume do not contribute much in modifying B of α-Fe. Figure 5(c) shows that the calculated B_{mf} are in a rather good positive correlation with experimental B of solutes in pure states [53], which agrees with the reported positive correlation between the calculated B of fcc Ni based, fcc Al based, and hcp Mg based solid solutions, and experimental B values of pure solutes [21, 22, 29].

In order to explain what is behind the positive correlation between B of pure solutes and B_{mf}, we calculate the valence electron density n_{WS} in bcc Fe based solid solutions. We firstly calculate B with PAW-PW91 functional for all elemental solids except for Mn [54], since its ground state, the noncollinear antiferromagnetic α-Mn, needs complicated initial settings and time-consuming computations to converge into the correct magnetic order [56]. Table 4 lists the PAW-PW91 B values of pure solutes where that of Mn is from Ref. [56] also calculated with PAW-PW91 functional [41, 58]. Figure 6(a) displays a good positive correlation between these theoretical B values of pure solutes and B_{mf} of Fe based solid solutions. From previous studies in Refs. [19–22, 27], it is reasonable that $B \sim n_{\mathrm{WS}}^2 V_{\mathrm{m}}$ is applicable to bcc $\mathrm{Fe}_{1-c}\mathrm{X}_c$ solid solutions. Similarly to Ref. [27], it is defined

$$n_{\mathrm{WS}} = ((1-c)n_{\mathrm{Fe}}V_{\mathrm{Fe}} + c n_{\mathrm{X}} V_{\mathrm{X}})/V_{\mathrm{m}}. \tag{6}$$

Herein, $n_{\mathrm{X}} = \sqrt{B_{\mathrm{X}}/V_{\mathrm{X}}}$ with B_{X}, V_{X} and n_{X} in units of GPa, $10^{-6}\mathrm{m}^3$/mole and e/au^3, respectively [20]. V_{Fe}, V_{X}, n_{Fe} and n_{X} can be calculated from theoretical results of lattice constants and B listed in Tables 3 and 4. If one takes partial derivative on both sides of the expression $B \sim n_{\mathrm{WS}}^2 V_{\mathrm{m}}$ with respect to solute content

c, there is

$$B_{mf} B_{\mathrm{Fe}} \sim \partial(n_{\mathrm{WS}}^2 V_{\mathrm{m}})/\partial c. \tag{7}$$

As shown in Fig. 6(b), the theoretical data of $\partial(n_{\mathrm{WS}}^2 V_{\mathrm{m}})/\partial c$ (divided by B_{Fe}) except that of Fe-Nb system can be perfectly fitted to the equation:

$$\partial(n_{\mathrm{WS}}^2 V_{\mathrm{m}})/\partial c = p_1 \exp(p_2 B_{mf}) + p_3. \tag{8}$$

The adjusted R^2 is 0.887, and the fitted values of p_1, p_2 and p_3 are 2.1, 0.268 and −1.241, respectively. Herein, for better display the exponential trend, the data of Fe-X (X=Re, Os and Ir) systems are included in Fig. 6(b). As shown in Fig. 7(a), the first-principles ΔB of Fe-X (X=Re, Os and Ir) systems all have gentler slope than that of Fe-W system, indicating larger B_{mf} than that of Fe-W system. Our results reveal an exponential, rather than linear, correlation between $\partial(n_{\mathrm{WS}}^2 V_{\mathrm{m}})/\partial c$ and B_{mf} in bcc Fe based solid solutions. Noticeably, n_{WS} is quite different from the concept of free electron density n_{free}, and the evidence is as following. Our calculated n_{WS} decreases with solute content c in all Fe-X systems. However, the first-principles Fermi energy ε_{F} increases with c in 10 Fe-X (X=Al, Cr, Ir, Mn, Mo, Os, Re, Si, V and W) systems. This means that n_{free} also increases with c, since ε_{F} scales as 2/3 power of n_{free}, according to free electron gas model. Hence, n_{WS} and n_{free} show opposite trends with solute conte c in these systems.

Let us then, discuss the mechanism of how solutes modify B of α-Fe. As common knowledge, B characterizes the compressibility of solids. For metallic systems, B is mainly determined by the kinetic energy of free electrons and the overlapping between bound-electron clouds around neighboring cations which contribute repulsion forces [44, 59]. Actually, the repulsion between overlapped bound-electron clouds can be attributed to increased kinetic energy of electrons in the overlapping area due to increased density. According to Thomas-Fermi statistics, the kinetic energy of electron cloud scales as 2/3 power of its density [59].

Hence, there is an inverse correlation between B and volume of metals. The general applicability of the empirical relation $n_{\mathrm{WS}} \sim \sqrt{B/V_{\mathrm{m}}}$ in elemental metals and in binary alloys [19–22, 27], illustrates that the so-called valence electron density at boundary of Wigner-Seitz cells, n_{WS}, perfectly represents the combination effects of free electron density and the overlapping between bound-electron clouds in a phenomenological way. From this point, it is convenient to discuss the electronic origin of solute effect on B of α-Fe by n_{WS}.

Figure 8(a) presents the n_{WS} on a Wigner-Seitz cell in α-Fe. Solute contributes free and bound electrons into the metallic solid solution, so that it directly changes n_{WS}; furthermore, solute can modulate n_{WS} by changing the volume. Figure 7(b) presents the first-principles Δa of Fe-X (X=Re, Os, Ir and W) systems versus solute content, indicating that their volumes are much expanded by adding solutes. Our calculated Ω_{sf} of solutes can be sorted into two classes. The first class includes solutes Ir, Mo, Nb, Os, Re and W, whose Ω_{sf} are fairly large, e.g., 0.628, 0.545 and 0.534 respectively for Ir, Os and Re. The second class contains all the other solutes, whose Ω_{sf} is much smaller than those of the first class, as shown in Fig. 5(b); for example, the greatest two Ω_{sf} values among the second class, are 0.37 and 0.296, respectively belonging to Ti and Ni. Solutes in the first class have much bigger volume-expanding effect than those in the second clase, leading to greater decrease of B. This explains the left shift of the half-filled symbols (representing solutes in the first class) from the short-dash line fitting to those filled symbols (representing solutes in the second class), and the exponential relation between $\partial(n_{\mathrm{WS}}^2 V_{\mathrm{m}})/\partial c$ and B_{mf} in Fig. 6(b). Hence, solutes modify B of α-Fe primarily via the valence electron density, n_{WS}, at boundary of Wigner-Seitz cells, including by modulating n_{WS} via volume. Table 5 lists the verified correlations between B of metallic solid solutions and other properties in previous studies and this work. Obviously, there exists similar correlation between n_{WS} and B in hcp

Mg-X (X=solutes) solid solution as those in other systems owing to the correlation between B and B_X. It is reasonable that good linear relation $n_\mathrm{WS}\sim\sqrt{B/V_\mathrm{m}}$ is unavailable in these metallic solid solutions because of the volume effect of solutes, as in our case of bcc Fe-X system.

4.3. Linear relation between Θ_{mf} and G_{mf}

Here we turn to discuss the correlations between solute effect on polycrystalline shear modulus G of α-Fe and other quantities. As shown in Fig. 9(a), Θ_{mf} increases in a perfect linear fashion with G_{mf} except for Fe-W system. The calculated Θ_{mf} of Fe-W system is much smaller for matching G_{mf}, which is attributed to the much heavier mass of W ion. However, if the mass of W was replaced by that of Fe in calculating Θ of Fe-W system, the resulted Θ_{mf} is right located on the fitting line, as shown by the open diamond symbol in Fig. 9(a). Ω_{sf} exhibits almost no correlation with G_{mf}, as shown in Fig. 9(b). These results indicate that the solute effect on bonding strength, rather than on volume, plays a dominant role in modifying G of α-Fe. This can be well understood from the "spring" representation of metallic bonds in α-Fe as shown in Fig. 8(b): all these bonds resist shear strain in a consistent manner. We also observe similar linear correlation between Θ_{mf} and E_{mf} as that between Θ_{mf} and G_{mf}, and no correlation between Ω_{sf} and E_{mf}. There is a weak positive correlation between G_{mf} and experimental G of pure solutes [53], as shown in Fig. 9(c). E_{mf} also show a weak positive correlation with experimental E of pure solutes.

Hu *et al.* found that the shear modulus in [111] direction of bcc W based solid solutions, G_{111}, is in positive correlation with the W-X (X=solutes) bonding strength in [111] direction [27]. They reported that G_{111} of W-Mo solid solution is greater than that of other W-X (X=Ti, Pd) systems, which is corresponding to the higher charge density between adjacent W and Mo atoms in [111] direction than that between W and Ti (or Pb) atoms. They also reported that the theoretical G

values of bcc W based solid solutions, exhibit very weak correlation to equilibrium volume [27]. Their results are consistent with our calculations of Fe based solid solutions. As far as our reach, there has been no more report on the correlation between G and bonding strength in metallic solid solutions, as shown in Table 5. Nonetheless, the perfect linear relationship between G_{mf} and Θ_{mf} in bcc Fe-X system and the results in bcc W-X system [27] suggest that solutes modify G of bcc metals mainly via variation of bonding strength. Additionally, previous first-principles calculations indicate G of fcc Ni based solid solutions are in good negative correlation to equilibrium volume, which may need further study [21].

4.4. Correlation between G_{mf} and e/a

From above subsection, it is concluded that solutes modify G of α-Fe mainly by modulating electronic interactions between neighboring cations. Herein, we further discuss the case of 3d transition-metal solutes. Figure 10 plots G_{mf} versus electron-to-atom ratio e/a of 3d transition metals, which provides instructive information on how the electronic interactions between Fe and 3d solutes influence G of α-Fe. As it can be seen, G_{mf} approximately exhibits a linear increasing trend with e/a for early 3d metals up to Mn, but a linear decreasing trend for later ones from Co, so that the fitting lines present in a volcano's shape as a whole. This indicates that transition-metal solutes with similar number of valence electrons to iron form stronger bonding to bcc Fe solvent, leading to greater G. Hu *et al.* reported similar results for bcc W based solid solutions: an approximately linear increasing trend of G with the increasing number of valence electrons of early transition metals lying to the left of W in periodic table, but an approximately linear decreasing trend for later ones lying to the right of W [27]. Nonetheless, it should be noted that the increasing trend of G_{mf} versus e/a from Ti to Mn is opposite to the linear decreasing trend of $\partial G/\partial c$ versus e/a for Fe-X (X=3d transition-metal solutes) systems in Ref. [28]. This discrepancy might be due to structural difference

between the bcc Fe based solid solutions with uniform-distributed solutes in our modelling, and real materials, in which solutes almost always exist in short-range order [42].

5. Summary

Based on first-principles calculations within the density functional theory, the changes of elastic moduli (ΔB, ΔG and ΔE) owing to solutes, are calculated for 12 bcc Fe based homogeneous solid solutions within solute content c from 0.4 at.% to 1.85 at.%. Results show that these elastic moduli decrease linearly with c in 11 Fe-X (X=Ti, V, Nb, Cr, Mo, W, Co, Ni, Cu, Al and Si) systems. For Fe-Mn system, ΔB show a nonlinear increase at 1.39 at. % Mn, while ΔG and ΔE increase linearly with Mn content. It is found that the nonlinear variation of ΔB in Fe-Mn system originates from the change in electronic environment around solute Mn rather than in magnetic moment of solute Mn. It is concluded that the elastic moduli of bcc Fe based solid solutions are in linear solute-content dependence on the condition of unchanged electronic environment of bcc Fe solvent, and vary nonlinearly once sufficient solutes change the electronic environment of the solvent.

In this paper, an elastic modulus factor κ_{mf} is defined to characterize solute effect on the elastic modulus κ of α-Fe. The "modulus" factor of Debye temperature, Θ_{mf}, is proposed to characterize solute effect on bonding strength of α-Fe. It is concluded that solutes modify B of α-Fe primarily via the valence electron density, n_{WS}, at boundary of Wigner-Seitz cells, and modify G via bonding strength. It is found that the theoretical $\partial(n_{\mathrm{WS}}^2 V_{\mathrm{m}})/\partial c$ increases exponentially with the bulk modulus factor B_{mf}, and Θ_{mf} increases linearly with G_{mf}. For 3d transition-metal solutes, G_{mf} increases linearly with electron-to-atom ratio e/a of solutes from Ti to Mn, but decreases linearly with e/a of solutes from Co to Cu, indicating that by adding solutes having similar valence electrons to iron leads to greater G of bcc

Fe based solid solutions. These results contribute new insights on the underlying mechanisms of how solutes modify elastic moduli of α-Fe.

Acknowledgments

Wei Liu would like to thank Zhijun Cheng and Jie Yao in Institute of Solid State Physics, Chinese Academy of Sciences for drawing pictures. This work is supported by the National Magnetic Confinement Fusion Program (Grant No. 2015GB112001), the National Natural Science Foundation of China (Nos: 51571187, 11475214, 11575229, 11505215, 11505214), and by the Center for Computation Science, Hefei Institutes of Physical Sciences. C.R. Miranda acknowledges the financial support provided by the Brazilian Ministry of Science and Technology for collaborative research between China and Brazil, and the Brazilian funding agencies National Council of Scientific and Technologic Development (CNPq), and Fundação de Amparo à Pesquisa do Estado de São Paulo (FAPESP).

References

[1] R.L. Klueh, D.S. Gelles, S. Jitsukawa, A. Kimura, G.R. Odette, B. van der Schaaf, M. Victoria, Ferritic/martensitic steels—overview of recent results, J. Nucl. Mater. 307-311 (2002) 455-465.

[2] L.K. Mansur, A.F. Rowcliffe, R.K. Nanstad, S.J. Zinkle, W.R. Corwin, R.E. Stoller, Materials needs for fusion, Generation IV fission reactors and spallation neutron sources—similarities and differences, J. Nucl. Mater. 329-333 (2004) 166-172.

[3] S.J. Zinkle, J.T. Busby, Structural materials for fission & fusion energy, Materials Today 12 (2009) 12-19.

[4] A.A.F. Tavassoli, E. Diegele, R. Lindau, N. Luzginova, H. Tanigawa, Current status and recent research achievements in ferritic/martensitic steels, J. Nucl. Mater. 455 (2014) 269-276.

[5] L. Tan, Y. Katoh, A.A.F. Tavassoli, J. Henry, M. Rieth, H. Sakasegawa, H. Tanigawa, Q. Huang, Recent status and improvement of reduced-activation ferritic-martensitic steels for high-temperature service, J. Nucl. Mater. 479 (2016) 515-523.

[6] W.J. Quadakkers, J. Piron-Abellan, V. Shemet, L. Singheiser, Metallic interconnectors for solid oxide fuel cells—a review, Mater. High Temp. 20 (2003) 115-127.

[7] J. Froitzheim, G.H. Meier, L. Niewolak, P.J. Ennis, H. Hattendorf, L. Singheiser, W.J. Quadakkers, Development of high strength ferritic steel for interconnect application in SOFCs, J. Power Sources 178 (2008) 163-173.

[8] N. Shaigan, W. Qu, D.G. Ivey, W. Chen, A review of recent progress in coatings, surface modifications and alloy developments for solid oxide fuel cell ferritic stainless steel interconnects, J. Power Sources 195 (2010) 1529-1542.

[9] J.C.W. Mah, A. Muchtar, M.R. Somalu, M.J. Ghazali, Metallic interconnects for solid oxide fuel cell: A review on protective coating and deposition techniques, Int. J. Hydrogen Energy 42 (2017) 9219-9229.

[10] D. Schmidt, M.C. Galetz, M. Schütze, Ferritic-martensitic steels: Improvement of the oxidation behavior in steam environments via diffusion coatings, Surf. & Coat. Tech. 237 (2013) 23-29.

[11] D. Fähsing, M. Rudolphi, L. Konrad, M.C. Galetz, Fireside Corrosion of

Chromium- and Aluminum-Coated Ferritic-Martensitic Steels, Oxid. Met. 88 (2017) 155-164.

[12] W. Liu, W.L. Wang, Q.F. Fang, C.S. Liu, Q.Y. Huang, Y.C. Wu, Concise relation of substitution energy to macroscopic deformation in a deformed system, Phys. Rev. B 84 (2011) 224101.

[13] T. Garnier, V.R. Manga, P. Bellon, D.R. Trinkle, Diffusion of Si impurities in Ni under stress: A first-principles study, Phys. Rev. B 90 (2014) 024306.

[14] T. Garnier, Z. Li, M. Nastar, P. Bellon, D.R. Trinkle, Calculation of strain effects on vacancy-mediated diffusion of impurities in fcc structures: General approach and application to $Ni_{1-x}Si_x$, Phys. Rev. B 90 (2014) 184301.

[15] W. Liu, X. Li, Y. Xu, C.S. Liu, Y. Liang, Electronic origin of strain effects on solute stabilities in iron, J. Appl. Phys. 120 (2016) 075902.

[16] A.M. Limarga, D.S. Wilkinson, Modeling the interaction between creep deformation and scale growth process, Acta Mater. 55 (2007) 189-201.

[17] Y.T. Zheng, F.Z. Xuan, Z. Wang, A dominant role of stress-dependent oxide structure on diffusion flux in the strain-reaction engineering, Chem. Phys. Lett. 626 (2015) 25-28.

[18] J.H. Rose, H.B. Shore, Elastic constants of the transition metals from a uniform electron gas, Phys. Rev. B 49 (1994) 11588-11601.

[19] A.R. Miedema, F.R. de Boer, P.F. de Chatel, Empirical description of the role of electronegativity in alloy formation, J. Phys. F: Met. Phys. 3 (1973) 1558-1576.

[20] C. Li, P. Wu, Correlation of bulk modulus and the constituent element properties of binary intermetallic compounds, Chem. Mater. 13 (2001) 4642-4648.

[21] D.E. Kim, S.L. Shang, Z.K. Liu, Effects of alloying elements on elastic properties of Ni by first-principles calculations, Comput. Mater. Sci. 47 (2009) 254-260.

[22] J. Wang, Y. Du, S.L. Shang, Z.K. Liu, Y.W. Li, Effects of alloying elements on elastic properties of Al by first-principles calculations, J. Min. Metall. Sect. B-Metall. 50 B (2014) 37-44.

[23] K. Chen, L.R. Zhao, J.S. Tse, Application of bond order in solid solution strengthening of nickel, J. Mater. Sci. Lett. 22 (2003) 603-605.

[24] T. Khmelevska, S. Khmelevskyi, A.V. Ruban, P. Mohn, Magnetism and origin of non-monotonous concentration dependence of the bulk modulus in Fe-rich alloys with Si, Ge and Sn: a first-principles study, J. Phys.: Condens. Matter 18 (2006) 6677-6689.

[25] A. Saengdeejing, Y. Chen, K. Suzuki, H. Miura, T. Mohri, First-principles study on the dilute Si in bcc Fe: Electronic and elastic properties up to 12.5 at.%Si, Comput. Mater. Sci. 70 (2013) 100-106.

[26] C.S. Kong, S.R. Broderick, T.E. Jones, C. Loyola, M.E. Eberhart, K. Rajan, Mining for elastic constants of intermetallics from the charge density landscape, Physica B 458 (2015) 1-7.

[27] Y.J. Hu, S.L. Shang, Y. Wang, K.A. Darling, B.G. Butler, L.J. Kecskes, Z.K. Liu, Effects of alloying elements and temperature on the elastic properties of W-based alloys by first-principles calculations, J. Alloys Compd. 671 (2016) 267-275.

[28] G. Ghosh, G.B. Olson, The isotropic shear modulus of multicomponent Fe-base solid solutions, Acta Mater. 50 (2002) 2655-2675.

[29] S. Ganeshan, S.L. Shang, Y. Wang, Z.K. Liu, Effect of alloying elements on the elastic properties of Mg from first-principles calculations, Acta Mater. 57 (2009) 3876-3884.

[30] Z.K. Liu, H. Zhang, S. Ganeshan, Y. Wang, S.N. Mathaudhu, Computational modeling of effects of alloying elements on elastic coefficients, Scripta Mater. 63 (2010) 686-691.

[31] D. Psiachos, T. Hammerschmidt, R. Drautz, *Ab initio* study of the modification of elastic properties of α-iron by hydrostatic strain and by hydrogen interstitials, Acta Mater. 59 (2011) 4255-4263.

[32] M.R. Fellinger, L.G. Hector Jr., D.R. Trinkle, *Ab initio* calculations of the lattice parameter and elastic stiffness coefficients of bcc Fe with solutes, Comput. Mater. Sci. 126 (2017) 503-513.

[33] W.C. Leslie, Iron and its dilute substitutional solid solutions, Metall. Trans. 3 (1972) 5-26.

[34] G.R. Speich, A.J. Schwoeble, W.C. Leslie, Elastic constants of binary iron-base alloys, Metall. Trans. 3 (1972) 2031.

[35] H.L. Zhang, B. Johansson, L. Vitos, *Ab initio* calculations of elastic properties of bcc Fe-Mg and Fe-Cr random alloys, Phys. Rev. B 79 (2009) 224201.

[36] H.L. Zhang, M.P.J. Punkkinen, B. Johansson, S. Hertzman, L. Vitos, Single-crystal elastic constants of ferromagnetic bcc Fe-based random alloys from first-principles theory, Phys. Rev. B 81 (2010) 184105.

[37] H.L. Zhang, M.P.J. Punkkinen, B. Johansson, L. Vitos, Theoretical elastic moduli of ferromagnetic bcc Fe alloys, J. Phys.: Condens. Matter 22 (2010) 275402.

[38] G. Kresse, J. Hafner, *Ab initio* molecular dynamics for liquid metals, Phys. Rev. B 47 (1993) 558-561(R); G. Kresse, J. Furthmüller, Efficient iterative schemes for *ab initio* total-energy calculations using a plane-wave basis set, Phys. Rev. B 54 (1996) 11169-11186.

[39] W. Liu, X. Wu, X. Li, C.S. Liu, Q.F. Fang, J.L. Chen, G.N. Luo, Z. Wang, Arithmetic extraction of elastic constants of cubic crystals from first-principles calculations of stress, Comput. Mater. Sci. 96 (2015) 117-123.

[40] H.M. Ledbetter, Estimation of Debye temperatures by averaging elastic coefficients, J. Appl. Phys. 44 (1973) 1451-1454.

[41] P. Olsson, T.P.C. Klaver, C. Domain, *Ab initio* study of solute transition-metal interactions with point defects in bcc Fe, Phys. Rev. B 81 (2010) 054102.

[42] I.A. Abrikosov, B. Johansson, Applicability of the coherent-potential approximation in the theory of random alloys, Phys. Rev. B 57 (1998) 14164-14173.

[43] H. Ishii, T. Kawarazaki, Y. Fujimura, Fatigue in binary alloys of bcc iron, Met. Trans. A 15 (1984) 679-691.

[44] W. Liu, Y. Xu, X. Li, X. Wu, C. S. Liu, Y. Liang, Z. Wang, First-principles study on stability of transition metal solutes in aluminum by analyzing the underlying forces, J. Appl. Phys. 117 (2015) 175901.

[45] Z. Chen, N. Kioussis, N. Ghoniem, D. Seif, Strain-field effects on the formation and migration energies of self interstitials in α-Fe from first principles, Phys. Rev. B 81 (2010) 094102.

[46] T.E. Cranshaw, C.E. Johnson, M.S. Ridout, The disturbance produced in an iron lattice by manganese atoms, Phys. Lett. 20 (1966) 97-99.

[47] Y. Koi, A. Tsujimura, T. Hihara, Nuclear magnetic resonances of Mn^{55} and V^{51} in dilute iron-base alloys, J. Phys. Soc. (Japan) 19 (1964) 1493-1494.

[48] V. Jaccarino, L.R. Walker, G.K. Wertheim, Localized moments of manganese impurities in ferromagnetic iron, Phys. Rev. Lett. 13 (1964) 752-754.

[49] M.F. Collins, G.G. Low, The magnetic moment distribution around transition element impurities in iron and nickel, Proc. Phys. Soc. 86 (1965) 535-548.

[50] H.W. King, Quantitative size-factors for metallic solid solutions, J. Mater. Sci. 1 (1966) 79-90.

[51] S.C. Abrahams, F.S.L. Hsu, Debye temperatures and cohesive properties, J. Chem. Phys. 63 (1975) 1162-1165.

[52] S.M. Dubiel, J. Cieślak, B.F.O. Costa, Debye temperature of disordered bcc Fe-Cr alloys, J. Phys.: Condens. Matter 22 (2010) 055402.

[53] ASM Handbook, Vol. 2, Properties and Selection: Nonferrous Alloys and Special-Purpose Materials, Ohio: ASM international, 1990, Chap. 4, Pure Metals.

[54] For all elemental crystals except Mn, the bulk modulus B is extracted from first-principles calculated stresses via an arithmetic scheme in Ref [39] by VASP with PW91 functional. Spin polarized calculations are performed for

AFM (antiferromagnetic) and FM (ferromagnetic) systems, while non spin-polarized calculations are performed for other systems. An energy cutoff of 350 eV is used for all systems. For elemental crystals in fcc and bcc structures except Cr, the primitive unit cell containing 1 atom with k-point mesh of $33*33*33$ is used in calculations, while a bcc unit cell containing 2 atoms with opposite magnetic moments with $23*23*23$ k-point mesh is used for bcc Cr AFM system. For elemental crystals in hcp structure, the primitive cell containing 2 atoms with k-point mesh of $25*25*17$ is used in calculations. For Si in diamond structure, the diamond cube cell containing 8 atoms with $11*11*11$ k-point mesh is used in calculations.

[55] N.W. Ashcroft, N.D. Mermin, Crystal lattices, in: Solid state physics, Thompson Learning Inc (1976), Beijing, World publishing corporation, reprint edition, 2004, pp. 63–84 (Chapter 4).

[56] D. Hobbs, J. Hafner, D. Spišák, Understanding the complex metallic element Mn: I. Crystalline and noncollinear magnetic structure of α-Mn, Phys. Rev. B 68 (2003) 014407.

[57] A.C. Lawson, A.C. Larson, M.C. Aronson, S. Johnson, Z. Fisk, P.C. Canfield, J.D. Thompson, R.B. Von Dreele, Magnetic and crystallographic order in α-manganese, J. Appl. Phys. 76 (1994) 7049-7051.

[58] J.P. Perdew, J.A. Chevary, S.H. Vosko, K.A. Jackson, M.R. Pederson, D.J. Singh, C. Fiolhais, Atoms, molecules, solids, and surfaces: Applications of the generalized gradient approximation for exchange and correlation, Phys. Rev. B 46 (1992) 6671-6687.

[59] K. Huang (original author), R.Q. Han (rewriter), Metallic bonding, in: Solid

state physics, Beijing, Higher eduation press, Chinese edition, 1988, pp. 67–68 (Chapter 2).

Figure Captions:

Fig. 1. (Color online) Changes of bulk modulus, polycrystalline shear modulus and Young's modulus, ΔB, ΔG and ΔE (left panel), and lattice constant change Δa, Debye temperature change $\Delta\Theta$ (right panel) of bcc Fe-X (X= early transition metals) sold solutions; the abscissa is solute content. Lines are linear fits.

Fig. 2. (Color online) Changes of bulk modulus, polycrystalline shear modulus and Young's modulus, ΔB, ΔG and ΔE (left panel), and lattice constant change Δa, Debye temperature change $\Delta\Theta$ (right panel) of bcc Fe-X (X=later transition metals, Al, and Si) systems; the abscissa is solute content; all the scales are the same as those in Fig. 1. Lines are linear fits.

Fig. 3. (Color online) Differential charge density on the (110) plane in bcc Fe-Mn solid solution with Mn content 1.04 at. % (left panel) and 1.39 at. % (right panel). In both pictures Mn atoms are placed at the center. The unit of charge density is $e/\text{Å}^3$.

Fig. 4. (Color online) (a) Averaged magnetic moments of the first and second nearest neighboring (1nn and 2nn) shells of Fe atoms around Mn, and farther Fe atoms, and (b) magnetic moment of solute Mn in bcc Fe-Mn solid solution at different Mn contents; (c) lattice constant change Δa, and (d) changes of single-crystal elastic moduli ΔC_{11}, ΔC_{12} and ΔC_{44} and bulk modulus change ΔB of bcc Fe-Mn solid solution at different Mn contents.

Fig. 5. (Color online) (a) "Modulus" factor of Debye temperature Θ_{mf}, (b) volume size factor Ω_{sf}, and (c) experimental bulk modulus B of pure solutes versus bulk modulus factor B_{mf} of bcc Fe-X (X= 12 solutes) systems. B_{mf} of Fe-Mn system

is calculated in the range from 0.4 to 1.04 at.% Mn.

Fig. 6. (Color online) First-principles results of (a) bulk modulus B of pure solutes and (b) $\partial(n_{\mathrm{WS}}^2 V_{\mathrm{m}})/\partial c$ (see the text for a description) versus bulk modulus factor B_{mf} of bcc Fe-X (X= 15 solutes) systems. B_{mf} of Fe-Mn system is calculated in the range from 0.4 to 1.04 at.% Mn. Solid curve is exponential fit to filled and half-filled symbols; short-dash line is linear fit to filled symbols.

Fig. 7. (Color online) (a) lattice constant change Δa and (b) bulk modulus change ΔB versus solute content for bcc Fe-X(X= Ir, Os, Re and W) solid solutions.

Fig. 8. (Color online) (a) Charge density on a Wigner-Seitz cell in a bcc cell of α-Fe. The lower two hexagons are darkened to improve stereoscopic impression. The dash lines are body diagonals. The unit of charge density is $e/\text{Å}^3$. (b) "Spring" representation of metallic bonding in a bcc cell of α-Fe.

Fig. 9. (Color online) (a) "Modulus" factor of Debye temperature Θ_{mf}, (b) volume size factor Ω_{sf}, and (c) experimental polycrystalline shear modulus G of pure solutes versus the polycrystalline shear modulus factor G_{mf} of bcc Fe-X (X= 12 solutes) systems. In panel (a), the vertical coordinate of the open diamond symbol marked by W* is the Θ_{mf} value of Fe-W system calculated by replacing the mass of W with that of Fe; the line is a linear fit to the data except those of Fe-W system.

Fig. 10. Polycrystalline shear modulus factor G_{mf} versus electron-to-atom ratio e/a of 3d transition-metal solutes. Lines are linear fits. The electronic configurations of 3d transition metals in ground state are shown.

Table 1: Atomic percent concentrations of solutes (at.%), supercells (in multiples *l*, *m* and *n* of a two-atom bcc Fe cell respectively along [100], [010] and [001] directions) and *k*-point meshes of five model systems. Herein X denotes solute; *l*, *m* and *n* are integers.

system	at.% X	supercell	*k*-point mesh
$Fe_{249}X_1$	0.40	5×5×5	4∗4∗4
$Fe_{127}X_1$	0.78	4×4×4	5∗5∗5
$Fe_{95}X_1$	1.04	4×4×3	5∗5∗7
$Fe_{71}X_1$	1.39	3×3×4	7∗7∗5
$Fe_{53}X_1$	1.85	3×3×3	7∗7∗7

Table 2: Components (%) of HS1, HS2, NS1 and SS89 strains.

HS1 (e_{H1})	HS2 (e_{H2})	NS1 (e_{11}, e_{22}, e_{33})	SS89 (e_{11}, e_{33}, e_{12})
0.15	−0.15	−0.99, 1.0, 0	0.004, 0, 0.873

Table 3: Lattice constant a_0 (Unit: Å), polycrystalline elastic moduli B, E and G (Unit: GPa) and Debye temperature Θ (Unit: K) of α-Fe calculated by different group of supercells and k-point meshes.

system	a_0	B	E	G	Θ	supercell	k-point mesh
Fe_{250}	2.8303	191.50	214.54	81.68	468.57	5×5×5	4∗4∗4
Fe_{128}	2.8305	192.00	214.61	81.68	468.61	4×4×4	5∗5∗5
Fe_{96}	2.8300	193.50	215.76	82.09	469.78	4×4×3	5∗5∗7
Fe_{72}	2.8297	195.00	216.15	82.71	471.53	3×3×4	7∗7∗5
Fe_{54}	2.8292	195.17	218.68	83.26	472.99	3×3×3	7∗7∗7

Table 4: Lattice constant a (and c for tet and hcp structures; Unit: Å) and bulk modulus B (Unit: GPa) of elemental crystals calculated in this paper [54]. Herein tet and dia are abbreviated for tetragonal and diamond structures, respectively. AFM and FM are abbreviated for antiferromagnetic and ferromagnetic phases, respectively. Experimental (exp.) values are also listed for comparison.

elemental crystal	a, c (PW91)	a, c (exp.)[a]	B (PW91)	B (exp.)[b]
V bcc	2.9766	3.02	188.33	158
Nb bcc	3.3202	3.30	182.56	170
Cr bcc AFM	2.8482	2.88	196.67	160
Mo bcc	3.1703	3.15	249.67	261
W bcc	3.1740	3.16	312.0	311
Ir fcc	3.8789	3.84	345.67	371
Ni fcc FM	3.5229	3.52	192.56	177
Cu fcc	3.6285	3.61	133.11	138
Al fcc	4.0465	4.05	74.78	75.2
Si dia	5.4665	5.43	89.11	98
Mn tet AFM	8.669, 8.668[c]	8.877, 8.873[d]	188[c]	92.6
Ti hcp	2.9195, 4.6195	2.95, 4.69	122.56	108
Re hcp	2.7774, 4.4832	2.76, 4.46	371.17	334
Os hcp	2.7588, 4.3512	2.74, 4.33	401.83	373
Co hcp FM	2.4862, 4.0169	2.51, 4.07	207.67	182

[a]Ref. [55] [b]Ref. [20] [c]Ref. [56] [d]Ref. [57]

Table 5: Correlations of B and G of metallic solid solutions with other properties. $n_{\rm WS}$ is valence electron density at boundary of Wigner-Seitz cells and V is volume of metallic solid solutions. BS is the acronym for Bonding Strength. $B_{\rm X}$ and $G_{\rm X}$ are bulk and polycrystalline shear moduli of solute X, respectively. √ and × denote that correlation exists and do not exist, respectively; ✓✓ denotes quantitative relationship.

	$n_{\rm WS}$	V	$B_{\rm X}$		BS	V	$G_{\rm X}$
B(fcc Ni-X) [21]	√	–	√	G(fcc Ni-X) [21]	–	√	–
B(fcc Al-X) [22]	√	√	–	G(bcc W-X) [27]	√	×	–
B(bcc W-X) [27]	√	√	√	G(bcc Fe-X) [28]	×	√	–
B(hcp Mg-X) [29]	–	√	√	G(hcp Mg-X) [29]	–	–	√
B(bcc Fe-X) [ours]	✓✓	×	√	G(bcc Fe-X) [ours]	✓✓	×	×

Figure 1

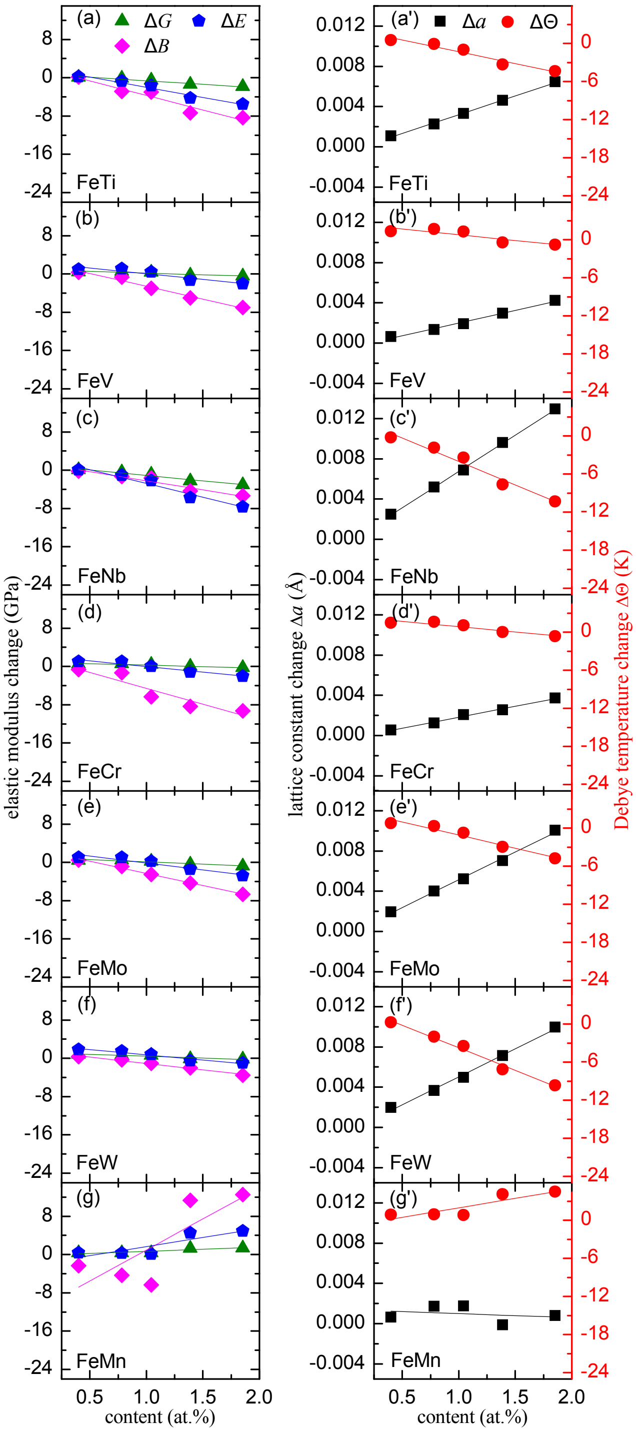
(a) ΔG ΔE ΔB
(a') Δa ΔΘ
FeTi
(b)
(b')
FeV
(c)
(c')
FeNb
(d)
(d')
FeCr
(e)
(e')
FeMo
(f)
(f')
FeW
(g)
(g')
FeMn
elastic modulus change (GPa)
lattice constant change Δa (Å)
Debye temperature change ΔΘ (K)
content (at.%)
content (at.%)

Figure 2

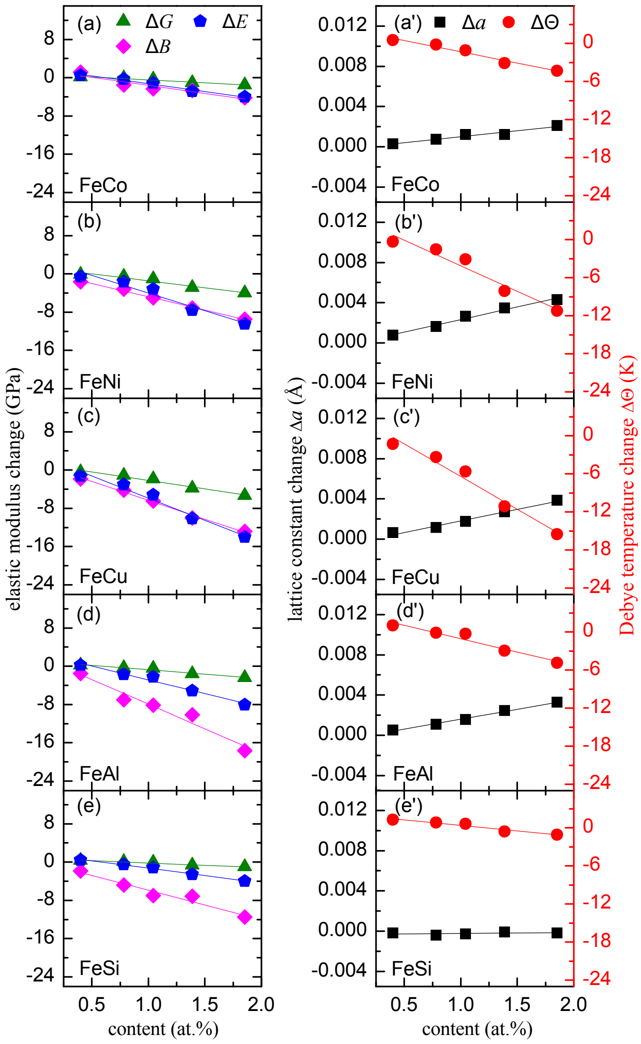

(a)
ΔG
ΔE
ΔB
FeCo
(b)
FeNi
(c)
FeCu
(d)
FeAl
(e)
FeSi
elastic modulus change (GPa)
content (at.%)
(a')
Δa
ΔΘ
(b')
(c')
(d')
(e')
lattice constant change Δa (Å)
Debye temperature change ΔΘ (K)
content (at.%)

Figure 3

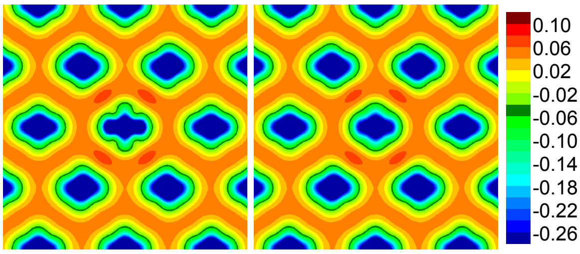

Figure 4

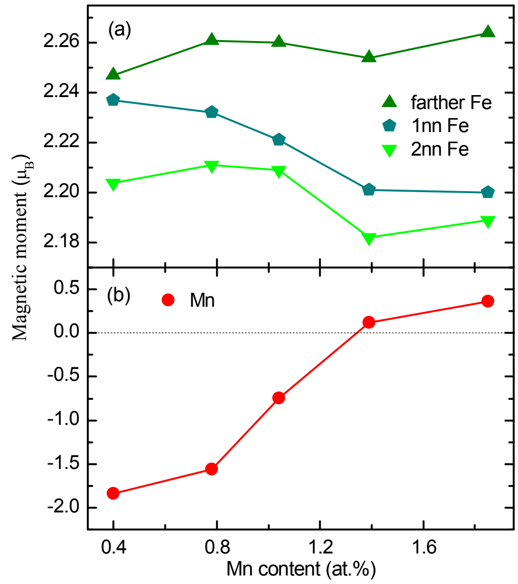

(a)
farther Fe
1nn Fe
2nn Fe
Magnetic moment (μ_B)
2.26
2.24
2.22
2.20
2.18
(b)
Mn
0.5
0.0
-0.5
-1.0
-1.5
-2.0
0.4
0.8
1.2
1.6
Mn content (at.%)

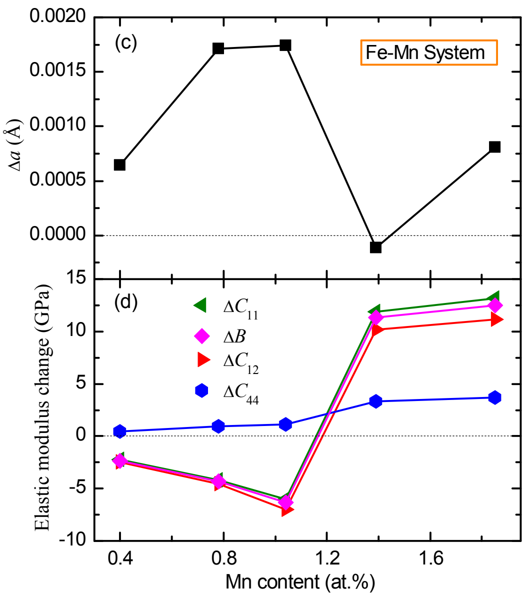

(c)
Fe-Mn System
Δa (Å)
0.0020
0.0015
0.0010
0.0005
0.0000
(d)
ΔC_{11}
ΔB
ΔC_{12}
ΔC_{44}
Elastic modulus change (GPa)
15
10
5
0
-5
-10
0.4
0.8
1.2
1.6
Mn content (at.%)

Figure 5

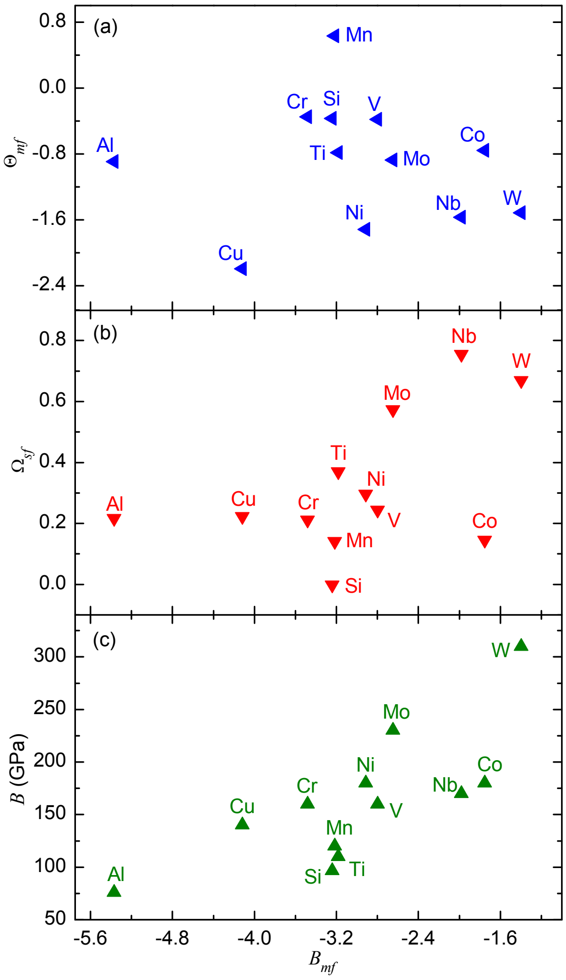
(a)
Mn
Cr
Si
V
Co
Al
Ti
Mo
Ni
Nb
W
Cu
0.8
0.0
-0.8
-1.6
-2.4
Θ_{mf}
(b)
Nb
W
Mo
Ti
Ni
Al
Cu
Cr
V
Co
Mn
Si
0.8
0.6
0.4
0.2
0.0
Ω_{sf}
(c)
W
Mo
Ni
Co
Cr
Nb
Cu
V
Mn
Al
Si
Ti
300
250
200
150
100
50
B (GPa)
-5.6
-4.8
-4.0
-3.2
-2.4
-1.6
B_{mf}

Figure 6

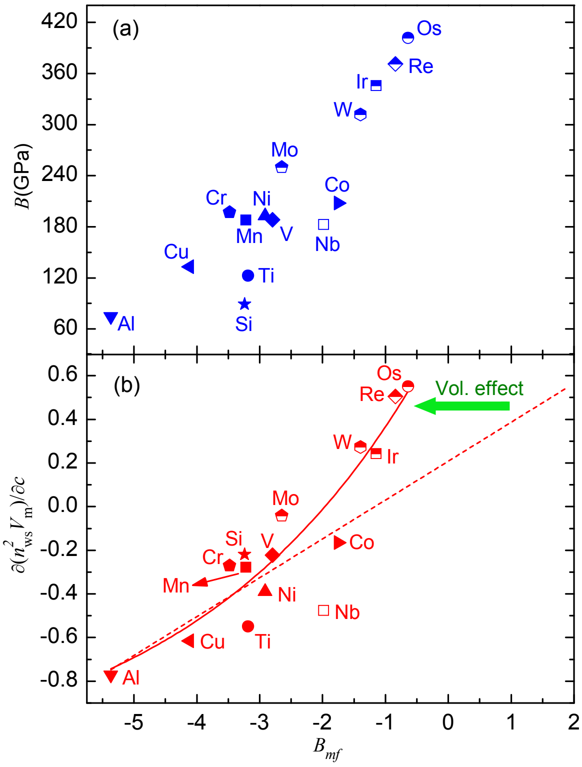

(a)
B(GPa)
420
360
300
240
180
120
60
Os
Re
Ir
W
Mo
Co
Cr
Ni
Mn
V
Nb
Cu
Ti
Al
Si
(b)
$\partial(n_{ws}^2 V_m)/\partial c$
0.6
0.4
0.2
0.0
-0.2
-0.4
-0.6
-0.8
Os
Re
Vol. effect
W
Ir
Mo
Si
V
Cr
Co
Mn
Ni
Nb
Cu
Ti
Al
-5
-4
-3
-2
-1
0
1
2
B_{mf}

Figure 7

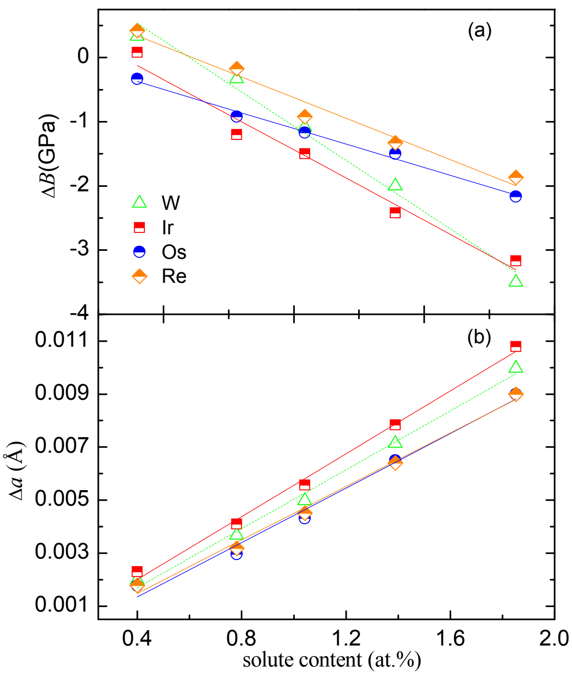

(a)
0
-1
-2
-3
-4
ΔB(GPa)
W
Ir
Os
Re
(b)
0.011
0.009
0.007
0.005
0.003
0.001
Δa (Å)
0.4
0.8
1.2
1.6
2.0
solute content (at.%)

Figure 8

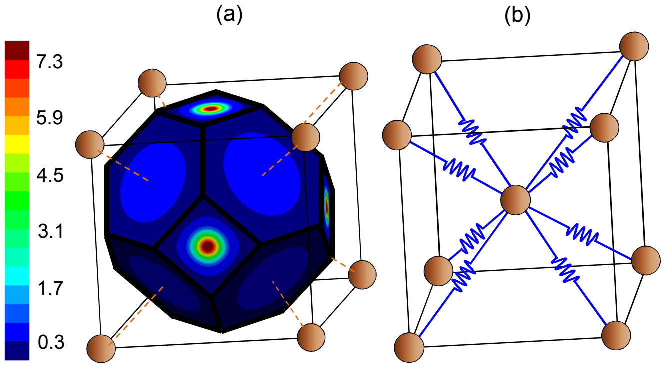

Figure 9

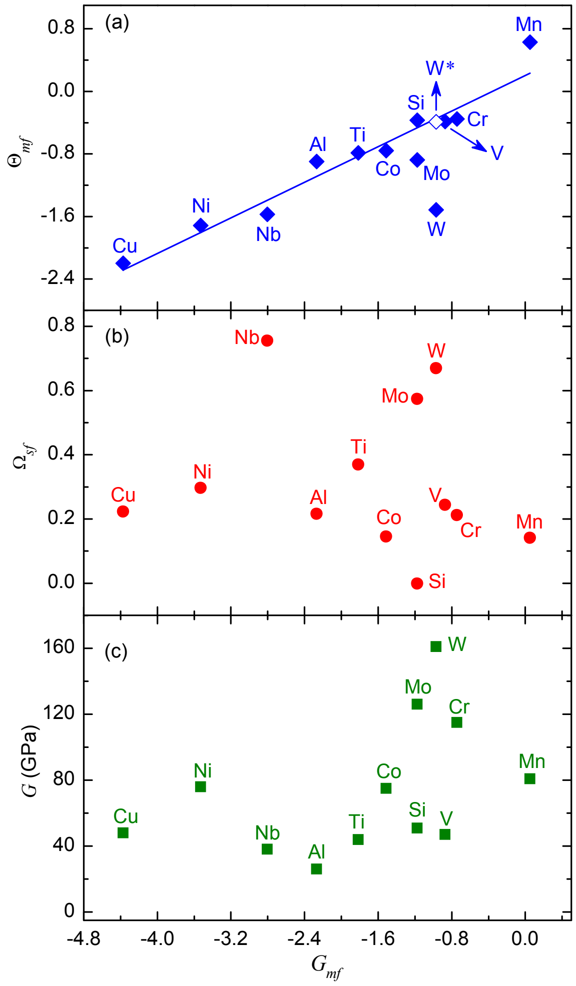

Figure 10

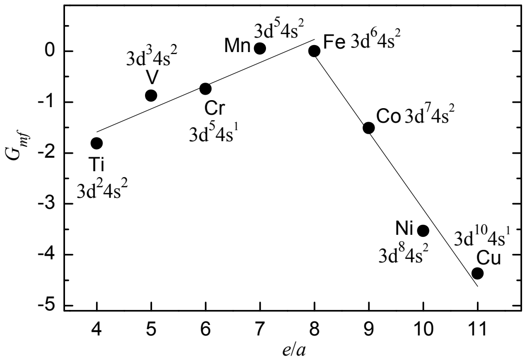

G_{mf}
e/a
Ti
$3d^2 4s^2$
V
$3d^3 4s^2$
Cr
$3d^5 4s^1$
Mn
$3d^5 4s^2$
Fe
$3d^6 4s^2$
Co
$3d^7 4s^2$
Ni
$3d^8 4s^2$
Cu
$3d^{10} 4s^1$